

Particle Spectra in the Integrated Hydrokinetic Model at RHIC BES Energies

Narendra Rathod,¹ Yuri Sinyukov,^{2,1} Musfer Adzhymambetov,^{2,*} and Hanna Zbroszczyk¹

¹*Warsaw University of Technology, Faculty of Physics, Koszykowa 75, 00-662 Warsaw, Poland*

²*Bogolyubov Institute for Theoretical Physics, Metrolohichna 14b, 03143 Kyiv, Ukraine*

(Dated: June 18, 2025)

This paper focuses on the description and prediction of particle production in Au+Au collisions at various center-of-mass energies ($\sqrt{s_{NN}} = 7.7, 11.5, 14.5, 19.6, 27.0$, and 39.0 GeV), using the Integrated HydroKinetic model (iHKM). The iHKM, initially created for description of ultrarelativistic nucleus-nucleus collisions, has been extended to cover intermediate and low relativistic energies, ranging from 2.5 to 50 GeV per colliding nucleon pair, and in cases where this distinction is needed, we refer to the modified version as iHKMe. The study explores the sensitivity of model predictions to variations in key parameters, including the relaxation time and thermalization degree during the prethermal stage, as well as the nature of the equation of state transition in the hydrodynamic phase. The iHKM successfully reproduces experimental results from the STAR experiment within the RHIC Beam Energy Scan program, with particular emphasis on midrapidity ($|y| < 0.1$) observables such as particle multiplicity densities (dN/dy), average transverse momenta ($\langle p_T \rangle$), and particle yield ratios. In addition, the paper examines the evolution of chemical and kinetic freeze-out across different collision energies and centrality classes. These results offer a consistent description of the collective properties of strongly interacting matter formed in heavy-ion collisions, spanning a wide range of energies and baryon chemical potentials at RHIC.

I. INTRODUCTION

It is widely considered that relativistic heavy-ion collisions, such as those conducted at the Large Hadron Collider (LHC) and the Relativistic Heavy Ion Collider (RHIC), create new forms of strongly interacting matter. Under extreme temperatures and densities, deconfined quarks and gluons can form a nearly equilibrated state known as the quark-gluon plasma (QGP) [1]. In contrast, under normal Earth conditions, quarks and gluons are confined within color-neutral hadrons due to the phenomenon of confinement.

In the quantum chromodynamics (QCD) phase diagram, the QGP and the hadron-resonance gas (HRG) phases are connected via a smooth crossover transition at vanishing baryon chemical potential [2], a scenario realized in collisions at LHC energies and the top RHIC energies. However, at higher baryon densities, the system is expected to undergo a genuine phase transition, potentially of first order [3, 4]. If such a phase transition line exists in the QCD phase diagram, it must end at a critical point, beyond which the transition becomes a crossover. Ongoing and upcoming experiments at lower collision energies, typically in the range of several GeV per nucleon pair, aim to identify clear signals of this phase transition and locate the critical endpoint.

With the launch of the Beam Energy Scan (BES) program at RHIC, three primary objectives were outlined [5]. The first goal is to explore the QCD phase diagram by varying the center-of-mass collision energy, $\sqrt{s_{NN}}$, in the range from 7.7 to 39 GeV. This variation enables access to different regions of temperature T and baryon

chemical potentials μ_B during the system's evolution, facilitating the search for the onset of deconfinement. The second goal is to investigate fluctuations and enhanced susceptibilities that are expected to increase near the QCD critical point [6–8]. However, such critical signatures may be suppressed due to conservation laws and the finite size and lifetime of the system. This challenge leads to the third goal: to identify observables sensitive to the softening of the QCD equation of state (EoS), which may signal the presence of a first-order phase transition.

One of the main challenges in analyzing and interpreting experimental results from heavy-ion collisions stems from the complex and dynamic evolution of the system, combined with its small spatial extent and extremely short lifetime. The properties of strongly interacting matter, particularly its behavior near a potential phase transition or critical point, affect experimental observables only indirectly. To extract these effects quantitatively, or even estimate them qualitatively, it is often necessary to construct a comprehensive dynamical model that simulates the system's entire evolution, from the initial impact to the final detection of produced hadrons.

Relativistic hydrodynamics has emerged as the most effective framework for describing the collective expansion of the strongly interacting matter created in these collisions. However, it comes with notable limitations: it is primarily applicable to soft observables (low transverse momentum, p_T) and assumes local thermal equilibrium. To address these constraints, theorists have developed hybrid models that integrate relativistic hydrodynamics, used for the hot, dense equilibrated stage, with microscopic transport models that describe out-of-equilibrium dynamics. Such non-equilibrium conditions are expected both in the very early pre-equilibrium stage, before thermalization occurs, and in the late afterburner stage, when the system becomes dilute and departs from equilibrium

* adzhymambetov@gmail.com

due to expansion.

At the LHC and the highest RHIC energies, the standard model of heavy-ion collisions is well established and widely accepted [9]. This model typically divides the collision process into several distinct stages: the formation of a non-equilibrium state during the penetration of the colliding nuclei, subsequent thermalization process leading to formation of a quark-gluon plasma (QGP), hydrodynamic expansion of the resulting fireball, hadronization of the QGP into a hadron resonance gas (HRG), and finally, the hadronic cascade stage [10–15]. As the collision energy decreases, this overall picture remains qualitatively similar but becomes significantly more complex. First, the characteristic time for two gold nuclei to fully overlap is approximately 10^{-3} fm/c at $\sqrt{s_{NN}} = 5.02$ TeV, while at $\sqrt{s_{NN}} = 14.5$ GeV at BES RHIC it exceeds 1.5 fm/c. As a result, the system becomes highly inhomogeneous, not only in the transverse but also in the longitudinal direction. Second, the lower energy density leads to a slower thermalization process, which may significantly shorten, or even eliminate the hydrodynamic phase. At collision energies of just a few GeV, it is plausible that the pre-equilibrium stage dominates the evolution, preventing the system from ever reaching full thermal equilibrium.

In a recent work [16], we proposed a novel framework to describe the full evolution of strongly interacting matter in relativistic heavy-ion collisions at intermediate and low energies, starting from the initial collision to the decoupling of free-streaming hadrons. In this extended version of the integrated hydrokinetic model, referred to as iHKMe, we adopt standard hydrodynamics to model the bulk evolution while simultaneously incorporating the UrQMD model to account for non-equilibrium dynamics. Unlike many hybrid approaches [17–20], which segment the evolution into distinct, sequential phases, iHKMe integrates microscopic and macroscopic descriptions concurrently across both equilibrium and non-equilibrium stages. In our approach, the system initially exists far from equilibrium and is gradually thermalized, transitioning into a hydrodynamic regime¹. Since the thermalization rate is not well constrained, it is treated as a free parameter in the model. By tuning this parameter, iHKMe enables a smooth interpolation between scenarios dominated by rapid thermalization (as at LHC energies) and those that remain largely non-equilibrated throughout the evolution, typical of low-energy collisions.

This study serves as a continuation of our previous work [16], in which we introduced an extended version of the integrated hydrokinetic model. In the present paper, we focus on describing the transverse momentum spectra of particles produced in Au-Au collisions at $\sqrt{s_{NN}} = 7.7 - 39$ GeV, as part of the RHIC Beam Energy Scan (BES) program. We calibrate the model's

free parameters using two different equations of state: one featuring a smooth crossover transition [22], and the other incorporating a first-order phase transition with a soft equation of state [23].

II. MODEL

The iHKM model was originally developed to study ultrarelativistic heavy-ion collisions [15]. We have recently extended the model to accommodate intermediate and low collision energies, broadening its applicability down to a few GeV. A detailed description of the extended model can be found in [16]. In this paper, we present a brief overview of the model's five evolutionary stages, discuss the possible overlap of these stages at lower collision energies, and introduce the key free parameters that control the model's dynamics.

1. Initial pre-equilibrium dynamics

One of the key differences between ultrarelativistic heavy-ion collisions at the LHC and the lower-energy experiments of the RHIC BES program lies in the very different relative velocities of colliding nuclei (and correspondingly space-time Lorentz factors for them), that, according to QCD approaches, leads to different physical pictures of nucleus-nucleus collisions at different energies. First, it concerns the different initial states for the colliding process. At TeV-scale energies, partons from the two nuclei interact only during the extremely short overlap time, approximately 10^{-3} fm/c, which is negligible compared to the full evolution timescale of the system (typically exceeding 10 fm/c). In contrast, at lower energies, the scenario becomes significantly more complex. The duration of the nuclear overlap, which increases with decreasing beam energy, can be estimated using the following equation:

$$\tau_{\text{overlap}} = \frac{2R_N}{\sqrt{(\sqrt{s_{NN}}/2m_N)^2 - 1}}, \quad (1)$$

where R_N is the radius of a nucleus and m_N is the nucleon mass. A straightforward calculation shows that at intermediate energies, around $\sqrt{s_{NN}} \sim 10$ GeV, the overlap time already exceeds 1.5 fm/c. Thermalization can only begin during this stage, meaning that a purely hydrodynamic description is not yet applicable. Consequently, a microscopic approach must be employed to model the early, out-of-equilibrium dynamics of the system.

In the iHKM for ultra-relativistic energies, the initial state of matter is generated using the Monte Carlo Glauber model, implemented in the GLISSANDO II package [24], featuring a longitudinally boost-invariant distribution in coordinate space and a highly anisotropic momentum distribution inspired by the Color Glass Condensate framework [25]. In the current version, event-by-

¹ Another approach to continuous transition from UrQMD to hydrodynamics is discussed in [21]

event UrQMD simulations are employed to describe the initial non-equilibrium dynamics up to a proper time τ_0 , which marks the onset of the thermalization stage, discussed in detail later.

The output of UrQMD simulations is used to construct a stress-energy tensor and baryon charge current, which are then used as initial conditions in the hydrodynamic equations. Summing over all particles (labeled with index i) within each proper time step $\Delta\tau$,

$$\left| \sqrt{t_i^2 - z_i^2} - \tau \right| < \Delta\tau/2, \quad (2)$$

we obtain

$$T_{\text{urqmd}}^{\mu\nu}(\tau; x_j) = \sum_i \frac{p_i^\mu p_i^\nu}{p_i^0} \mathcal{K}_{ij}, \quad (3)$$

$$J_{\text{urqmd}}^\mu(\tau; x_j) = \sum_i B_i \frac{p_i^\mu}{p_i^0} \mathcal{K}_{ij}. \quad (4)$$

Here, $T_{\text{urqmd}}^{\mu\nu}$ represents the stress-energy tensor at proper time step τ_j , and $J_{\text{urqmd}}^\mu(\tau; x_j)$ is the baryon current². Here, p_i^μ denotes the four-momentum of particle i , and B_i represents its baryon charge. We also utilize a \mathcal{K}_{ij} for particle smearing to generate a relatively smooth or averaged over the ensemble of similar events tensors.

$$\mathcal{K}_{ij} = \frac{n_j^\lambda u_{i\lambda}}{(\pi R^2)^{3/2}} \exp\left(\frac{r_{ij}^\mu (g_{\mu\nu} - u_\mu^i u_\nu^i) r_{ij}^\nu}{R^2}\right). \quad (5)$$

. In this expression, $r_{ij}^\mu = x_i^\mu - x_j^\mu$ represents the radius vector between the particle and the center of the cell ($x_i, x_j \in \sigma^\mu$), $u_{i\lambda}$ is four-velocity of particle, and n_j^λ is a normal vector to the hypersurface on the lattice $\Delta\sigma^\mu$

$$\Delta\sigma^\mu = n^\mu \Delta x \Delta y \Delta \eta, \quad (6)$$

$$n^\mu = (\tau \cosh \eta, 0, 0, \tau \sinh \eta), \quad (7)$$

In Eq. (5), a free scalar parameter of the model R is introduced. It is responsible for the smoothness of the initial collisions. Lastly, let us specify that $\sum_j \mathcal{K}_{ij} = 1$, ensuring no noticeable violations of conservation laws in this procedure.

2. Thermalization

During the thermalization stage, the system is assumed to consist of two coexisting phases. The first is a non-equilibrium component that evolves according to the UrQMD model and is described by Eq. (3). The second

represents near-equilibrium matter governed by relativistic hydrodynamics. Its tensors can be written as follows

$$T_{\text{hydro}}^{\mu\nu}(x) = (\epsilon + p) u^\mu u^\nu - p g^{\mu\nu} + \pi^{\mu\nu}. \quad (8)$$

$$J_{\text{hydro}}^\mu(x) = n_B u^\mu, \quad (9)$$

where ϵ , p , and n_B represent the local energy density, pressure, and baryonic density, respectively. u^μ denotes the four-velocity of the fluid, $g^{\mu\nu}$ is the metric tensor, and $\pi^{\mu\nu}$ stands for the shear-stress tensor. The energy density, baryon density, and pressure are connected through the equation of state:

$$p = p(\epsilon, n_B). \quad (10)$$

A linear combination of two components gives the total tensors of the system:

$$T_{\text{total}}^{\mu\nu}(x) = T_{\text{urqmd}}^{\mu\nu}(x) \cdot \mathcal{P}_\tau + T_{\text{hydro}}^{\mu\nu}(x) \cdot (1 - \mathcal{P}_\tau), \quad (11)$$

$$J_{\text{total}}^\mu(x) = J_{\text{urqmd}}^\mu(x) \cdot \mathcal{P}_\tau + J_{\text{hydro}}^\mu(x) \cdot (1 - \mathcal{P}_\tau), \quad (12)$$

where $\mathcal{P}_\tau = \mathcal{P}(\tau)$ is a weight function such that $\mathcal{P}(\tau_0) = 1$ at the start of the thermalization stage, $\mathcal{P}(\tau_{th}) = 0$ at the end, and $0 < \mathcal{P}(\tau_0 < \tau < \tau_{th}) < 1$ in between. So this weight function regulates how matter is pumped from one component to another during the thermalization. As in our previous papers [26, 27] we utilize an ansatz for $\mathcal{P}(\tau)$ inspired by the Boltzmann equation in relaxation time approximation.

$$\mathcal{P}(\tau) = \left(\frac{\tau_{th} - \tau}{\tau_{th} - \tau_0} \right)^{\frac{\tau_{th} - \tau_0}{\tau_{rel}}}. \quad (13)$$

This function involves three free parameters: the onset of thermalization τ_0 , end of thermalization τ_{th} , and its speed encoded in relaxation time τ_{rel} .

3. Hydrodynamic expansion, particlization, and hadron cascade

After thermalization is achieved, iHKM follows a classical path of hybrid models. At τ_{th} , the system expands via viscous hydrodynamic equations, which we solve numerically using the vHLLE code [28]. Once the system becomes dilute and reaches the critical energy density ϵ_{sw} , the evolution switches back to the UrQMD cascade. To determine the particlization hypersurface of constant energy density, we employ the Cornelius routine [29, 30]. The particlization of liquid into hadron resonant gas is realized via a Cooper-Frye-like algorithm

$$N^i = \int d^3p \int \frac{d\sigma_\mu p^\mu}{p_0} f_i(x, p). \quad (14)$$

² In this paper, we do not consider separate equations for other conserved charges. The electric charge density is assumed to be proportional to the baryon density, $n_q = \frac{Z}{A} n_b$, where $\frac{Z}{A} = 0.4$ for gold nuclei. The strangeness is always locally zero.

Here N^i is a number of hadrons of species i emitted from the element of hypersurface $d\sigma_\mu$ and $f_{i,eq}(x, p)$ is a distribution function. For high-energy collisions, the Bose-Einstein or Fermi-Dirac equilibrium distribution function with a small correction is a fairly good assumption. However, if the equilibrium is not reached, which we expect at several GeV experiments, two components must be considered. Following Eqs. (11), (12) in relaxation time approximation we obtain

$$f(x, p) = (1 - \mathcal{P}(\tau)) f_{eq.}(x, p) + \mathcal{P}(\tau) f_{n.eq.}(x, p), \quad (15)$$

where $f_{eq.}(x, p)$ is a near-equilibrium component constructed from the output of the hydrodynamic component, and $f_{n.eq.}(x, p)$ is a far from equilibrium distribution function constructed from UrQMD with a kernel (5).

III. FINETUNING AND RESULTS

1. Free parameters

To evaluate the sensitivity to the softening of the equation of state, we consider two qualitatively distinct models: the chiral EoS (CO) [22], which features a cross-over transition between the quark-gluon plasma and the hadron resonance gas, and an EoS with a first-order phase transition (PT) [23]. For each EoS, we perform simulations varying the free parameters as follows:

- τ_0 [fm/c] - start of the thermalization stage
- η/s [1] - shear viscosity to entropy density ratio. Scaling factor in shear stress tensor $\pi^{\mu\nu}$
- τ_{th} [fm/c] - end of the thermalization stage
- ϵ_{sw} [GeV/fm³] - hydrodynamic energy density corresponding to the transition to the hadron afterburner stage
- τ_{rel} [fm/c] - relaxation time
- R [fm] - gaussian smearing parameter in kernel (5)

To simplify the calibration procedure and reduce the number of free parameters, we fix the relaxation time to its maximum permitted value, effectively transferring all remaining flexibility to the parameter τ_{th} .

$$\tau_{rel} = \tau_{th} - \tau_0. \quad (16)$$

The Gaussian smearing parameter is fixed at a reasonable, though arbitrary, value of $R = 0.5$ fm for all initial conditions, as there is no clear physical justification for varying it between different experimental setups. Consequently, the smoothness of the initial state in our model is governed entirely by the thermalization stage. In summary, only four parameters, along with the choice of equation of state, are treated as free.

Parameter	Min Value	Max Value
τ_0 (fm/c)	0.8	2.2
τ_{rel} (fm/c)	0.3	2.0
η/s	0.0	0.2
ϵ_{sw} (GeV/fm ³)	0.35	0.55
R (fm)	0.4	1.2

TABLE I: Minimal and maximal allowed values of model parameters in Latin hypercube.

2. Sensitivity of spectra to the parameters

To explore the correlations between model parameters and observables, we generate 750 simulation sets for Au-Au collisions at $\sqrt{s_{NN}} = 14.5$ GeV within the 20 – 30% centrality class. The parameter values for each simulation are sampled using Latin hypercube sampling within the ranges specified in Table I. In this analysis, we allow variations in both the R and τ_{rel} parameters, while ensuring that the constraint given by Eq. (16) for τ_{th} .

For each parameter set, we generate 40 initial conditions using UrQMD. To improve statistical accuracy, we simulate 200 afterburner events on the particlization hypersurface for each initial condition, resulting in a total of 8,000 events per parameter set. We then construct transverse momentum spectra for pions, kaons, and (anti)protons. Fig. 1 shows the transverse momentum spectra at midrapidity, averaged over 750 parameter sets, with a one-standard-deviation range for both equations of state. On average, the midrapidity particle yields are higher in calculations with the softer phase-transition equation of state. However, this scenario also leads to weaker transverse flow, which is reflected in the high- p_T spectra. It is important to note that the mean values of the parameters listed in Table I do not correspond to the best-fit values for the experimental data. As a result, the spectra corresponding to the mean parameter set may lie outside the one-standard-deviation ranges shown (blue and red shaded bands) in Fig. 1.

Further, for simplicity, we consider only the following p_t bins: 0.15 ± 0.05 , 0.55 ± 0.05 , and 1.05 ± 0.05 GeV/c. For quantitative analysis, we use the Pearson correlation coefficient between the spectra values Y_i and the model parameters X_j :

$$P(X_j, Y_i) = \frac{\text{Cov}(X_j, Y_i)}{\sqrt{\text{Var}(X_j)\text{Var}(Y_i)}}. \quad (17)$$

Here, Cov is the covariance matrix, defined as

$$\text{Cov}(X_j, Y_i) = \frac{1}{N-1} \sum_{k=1}^N (X_{jk} - \mu_j^x) (Y_{ik} - \mu_i^y), \quad (18)$$

where the sum is taken over $N = 750$ simulation sets, and μ_j^x and μ_i^y are the mean values of the j^{th} parameter and the i^{th} observable, respectively. Finally, $\text{Var}(X_j)$ and

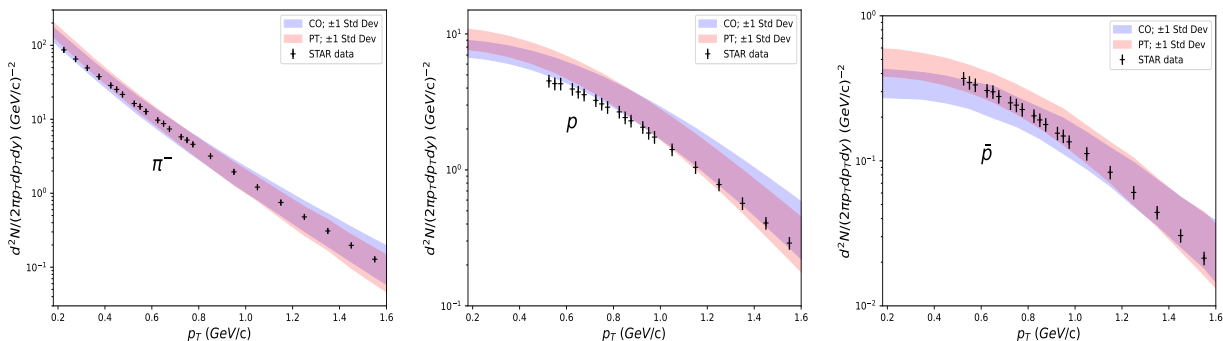


FIG. 1: p_T spectra for π^- , p , and \bar{p} (from left to right) averaged over 750 simulations, with one standard deviation from the mean values, using sets with random parameters within the ranges presented in Table I. Data correspond to Au+Au collisions at $\sqrt{s_{NN}} = 14.5$ GeV and 20-30% centrality class.

$\text{Var}(Y_i)$ are the diagonal elements of the self-covariance matrices $\text{Cov}(X_j, X_j)$ and $\text{Cov}(Y_i, Y_i)$, respectively.

The sign of the correlation matrix element indicates whether the parameter and observable are correlated (+) or anticorrelated³ (−), while the absolute value reflects the strength of the correlation, with “0” representing no correlation and “±1” corresponding to a strong (anti) correlation.

We construct correlation matrices for six particle species: π^\pm , K^\pm , p , and \bar{p} , using both equations of state. However, since the results for pions and kaons are very similar, Figure 2 presents only the correlations for negatively charged pions, protons, and antiprotons. Additionally, we show correlations only for antiprotons for the soft EoS with a first-order phase transition, as the results for all other cases are qualitatively and quantitatively similar to those of the crossover scenario.

One key conclusion from Figure 2 is that the common smoothing procedure for initial conditions (encoded in the parameter R) plays a crucial role in hydrodynamic simulations, which limits our ability to infer properties of strongly interacting matter in heavy-ion collisions. A second observation is that the parameter τ_{rel} behaves similarly to τ_0 , although its effect on the observables is less pronounced. We also find that, unlike other hadron species, antiproton yields are particularly sensitive to the switching energy density ϵ_{sw} , which marks the transition from hydrodynamics to transport. This sensitivity is also clearly demonstrated in [31]. It may be explained by the suppression of (anti)baryon yields in transport models like UrQMD [32, 33] or SMASH [34] used as afterburner on the final stage of the system’s evolution. This issue has been addressed in numerous papers to which we refer the reader [35–37].

When comparing the correlation matrices for antiprotons, we observe that in the case of a softer equation of

state (PT EoS), the parameters defining the pre-thermal evolution (i.e., τ_0 , τ_{rel} , R) play a more significant role than in the case of the crossover equation (CO EoS). This is reflected in the larger absolute values of the corresponding correlation coefficients. In contrast, the particlization energy density (ϵ_{sw}), which defines the late-stage evolution, becomes more influential when a stiffer equation of state is employed.

3. Model finetuning

In this study, we use particle spectra to calibrate the model’s free parameters. As shown in Fig. 2, the initiation of the thermalization stage, denoted by τ_0 , emerges as one of the most critical parameters. It is anticipated that in midrapidity, thermalization can begin even before the nuclei fully overlap, at τ_{overlap} (see Eq. (1)). Our numerical analysis indicates that the best agreement with experimental pion spectra is achieved when τ_0 is approximately $0.75\tau_{\text{overlap}}$. The conclusion of the thermalization phase has a significantly weaker influence on observables and, therefore, is determined with greater uncertainty. Nonetheless, it generally occurs at or slightly after the nuclei’ overlapping time.

The smoothing parameter R appears in various forms across most dynamical models with event-by-event fluctuating initial conditions, yet its value remains not well defined. For instance, paper[19] uses a value of 0.5 fm, Ref. [38] adopts 1 fm, and [39] treats it as a free parameter. In the iHKM model, the smoothing is further managed by the thermalization stage, and there is no strong evidence to vary this parameter across different collision energies. Therefore, we set R at the smallest reasonable value of 0.5 fm. Below this size, the initial particle distribution becomes too spiky, leading to instability in the initial hydrodynamic evolution.

Since low- p_T spectra show a weak dependence on η/s , we calibrate the viscosity by focusing on relatively high- p_T spectra (around 1 GeV/c) after fixing the thermalization stage parameters. Furthermore, we account for dif-

³ An increase in the parameter value leads to a decrease in the observable value.

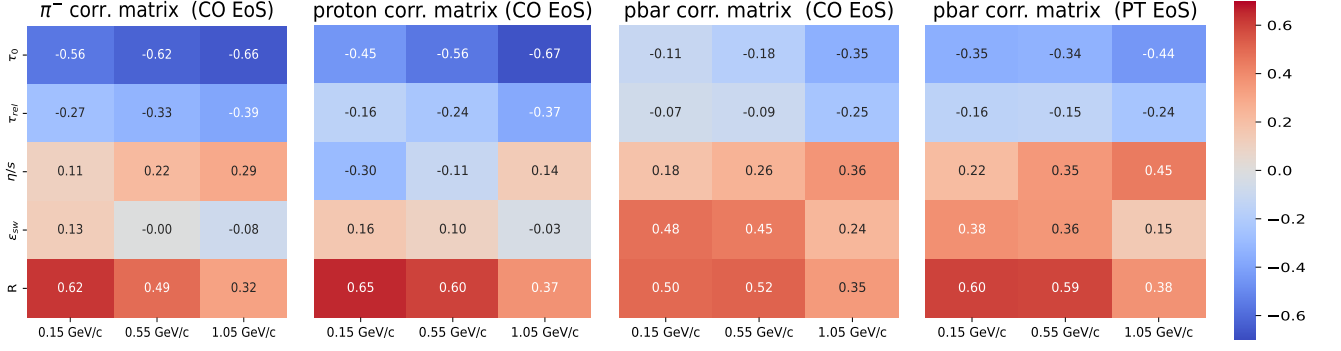


FIG. 2: Correlation coefficients between the five model parameters and the transverse momentum spectra at low, intermediate, and high p_T for π^- , p , and \bar{p} are presented. The results for π mesons and protons (shown in the two tables on the left) are very similar for both equations of state; therefore, only the crossover case is shown. For antiprotons (shown in the two plots on the right), we present the results for both scenarios.

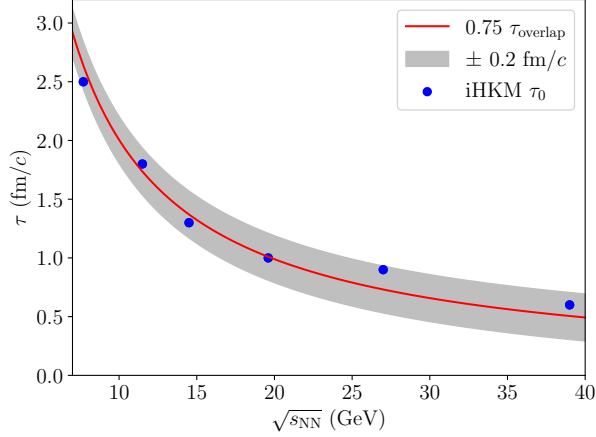


FIG. 3: Inferred τ_0 values vs nuclei overlapping time from Eq. (1) with 0.75 factor. The grey shaded zone reflects the estimated uncertainty of τ_0 for the crossover equation of state.

TABLE II: Parameters of iHKM providing the best description of bulk observables for Au+Au collisions at $\sqrt{s_{NN}} = 7.7, 11.5, 14.5, 19.6, 27.0, 39.0$ GeV.

$\sqrt{s_{NN}}$	EoS	R	τ_0	τ_{th}	η / s	ϵ_{sw}
7.7	PT	0.5	2.7	3.3	0.08	0.35
7.7	CO	0.5	2.5	3.3	0.08	0.50
11.5	PT	0.5	2.0	2.6	0.08	0.35
11.5	CO	0.5	1.8	2.6	0.08	0.50
14.5	PT	0.5	1.4	2.0	0.08	0.35
14.5	CO	0.5	1.3	2.3	0.08	0.50
19.6	PT	0.5	1.0	1.6	0.08	0.35
19.6	CO	0.5	1.0	1.6	0.08	0.50
27.0	PT	0.5	0.8	1.4	0.08	0.35
27.0	CO	0.5	0.8	1.4	0.08	0.50
39.0	PT	0.5	0.6	1.2	0.08	0.35
39.0	CO	0.5	0.6	1.6	0.08	0.50

ferences in the scale and slope of particle spectra when using different equations of state (see Fig.2). Because the antiproton spectra are particularly sensitive to η/s and ϵ_{sw} , we use experimental data for antiprotons to estimate these parameters. Although their values differ for the two equations of state, we keep them the same while varying the collision energy $\sqrt{s_{NN}}$.

4. Momentum spectra

In this section, we present the iHKM results for transverse momentum spectra in Au+Au collisions at energies of 7.7, 11.5, 14.5, 19.6, 27, and 39 GeV, across two centrality classes: 20-30% and 0-5%, as shown in Figs. 4 and 5. The final model parameters are summarized in Table II. The π^- spectra for the 20-30% centrality class were used to calibrate the model parameters. To improve the proton-to-antiproton ratio, the ϵ_{sw} parameter was allowed to change between different equations of state, but it was kept constant across collision energies. We also do not change model parameters for different centrality classes.

It is important to note that at RHIC BES, centrality classes are defined by the multiplicity of charged particles at midrapidity. In hydrodynamic simulations, using minimal-bias events for model calibration is inefficient. Therefore, we rely on the multiplicities of UrQMD events used for the initial conditions, extending them to longer times of up to 200 fm/c.

In Fig. 3, we demonstrate how our inferred value of τ_0 , derived from pion spectra, depends on the collision energy $\sqrt{s_{NN}}$. We found that it lies within a range of ± 0.2 fm/c from the value of $\tau_{overlap}$, scaled by a factor of 0.75. It is important to note that assuming thermalization begins at a fixed proper time τ is a simplification that may only be valid in the central region of the system. Upon analyzing the spectra presented in Figs. 5 and 4, several key trends emerge. First, the difference between the two equations of state is relatively small and becomes

negligible at higher collision energies. This behavior is also reflected in the model parameters listed in Table II.

Second, at midrapidity, the model consistently overestimates proton yields and underestimates antiproton yields across a wide range of transverse momenta. In extreme cases, the deviation between the model and experimental data can reach up to 40% at small transverse momenta p_T . Similar discrepancies in proton spectra have been reported in several other models [39–42], including those employing cascade-based initial conditions, such as SMASH [43] and UrQMD [33].

These discrepancies may stem from an imbalance between baryon creation and annihilation processes during the hadronic afterburner stage, or from an inaccurate baryon density distribution on the particlization hypersurface, leading to the over- or underproduction of baryons. In turn, the baryon densities on the particlization hypersurface are determined by the initial conditions (especially the baryon current) and the system’s subsequent evolution during the pre-equilibrium and hydrodynamic stages. However, the influence of these factors is beyond the scope of the present study.

It is also worth noting that in Ref. [44], the proton spectra show significantly better agreement with the experimental data at $\sqrt{s_{NN}} = 19.6$ GeV. This improvement, however, may result from the use of more flexible initial conditions, which introduce additional free parameters.

IV. SUMMARY

In this paper, we employ a recently developed, extended version of the iHKM model to describe the transverse momentum spectra of light hadrons in the Beam Energy Scan (BES) program at the Relativistic Heavy Ion Collider (RHIC). Our primary focus is to explore the relationship between the model’s free parameters and experimental observables. In particular, we investigate how variations in the thermalization time scales and the switching conditions between the hydrodynamic and hadronic stages influence particle spectra and transverse momentum distributions. Simulations are performed us-

ing the two distinct equations of state (EoS): one featuring a crossover transition in baryon-rich matter between quark-gluon plasma and hadron gas, and the other incorporating a first-order phase transition.

Our analysis reveals that the duration of the thermalization stage is approximately 1 fm/c across all RHIC BES energies in the range $\sqrt{s_{NN}} = 7.7\text{--}39$ GeV. However, thermalization begins earlier at lower collision energies. Specifically, our numerical results indicate that thermalization commences slightly before the two colliding nuclei fully overlap, assuming they propagate with their initial rapidities; this corresponds to $\tau_0 \approx 0.75 \tau_{\text{overlap}}$ for both considered equations of state.

We also find that both equations of state yield similarly accurate descriptions of the transverse momentum spectra when adjustments are made to the relaxation time scale. At higher collision energies within the BES range, differences between the results for spectra in the two scenarios become negligible. The analysis of elliptic flow is necessary.

The most pronounced difference between the two EoS scenarios emerges at $\sqrt{s_{NN}} = 7.7$ GeV, particularly in the yields of protons and kaons. This discrepancy is likely due to the differing trajectories the systems follow on the $T\text{--}\mu_B$ phase diagram during their evolution. The existence of a phase transition line, along with the choice of switching energy density ϵ_{sw} to the hadronic afterburner, plays a critical role in determining the parameters at chemical freeze-out. A more comprehensive analysis of additional bulk observables, especially of elliptic flow, within the iHKM framework is planned for future work.

ACKNOWLEDGMENTS

H.Z.’s work was supported by the Grant of National Science Centre, Poland, No: 2021/41/B/ST2/02409 and 2020/38/E/ST2/00019. The research of Yu. S. was partially funded by IDUB-POB projects granted by WUT (Excellence Initiative: Research University (ID-UB)). M.A. gratefully acknowledges support from the Simons Foundation (Grant SFI-PD-Ukraine-00014578).

-
- [1] E. V. Shuryak, Phys. Rept. **61**, 71 (1980).
 - [2] H.-T. Ding, F. Karsch, and S. Mukherjee, Int. J. Mod. Phys. E **24**, 1530007 (2015), arXiv:1504.05274 [hep-lat].
 - [3] M. A. Stephanov, Prog. Theor. Phys. Suppl. **153**, 139 (2004), arXiv:hep-ph/0402115.
 - [4] Z. Fodor and S. D. Katz, JHEP **04**, 050, arXiv:hep-lat/0402006.
 - [5] G. Odyniec, J. Phys. Conf. Ser. **455**, 012037 (2013).
 - [6] M. A. Stephanov, K. Rajagopal, and E. V. Shuryak, Phys. Rev. Lett. **81**, 4816 (1998), arXiv:hep-ph/9806219.
 - [7] M. A. Stephanov, K. Rajagopal, and E. V. Shuryak, Phys. Rev. D **60**, 114028 (1999), arXiv:hep-ph/9903292.
 - [8] P. C. Hohenberg and B. I. Halperin, Rev. Mod. Phys. **49**, 435 (1977).
 - [9] P. Romatschke, Int. J. Mod. Phys. E **19**, 1 (2010), arXiv:0902.3663 [hep-ph].
 - [10] B. Schenke, S. Jeon, and C. Gale, Phys. Rev. C **82**, 014903 (2010), arXiv:1004.1408 [hep-ph].
 - [11] C. Gale, S. Jeon, and B. Schenke, Int. J. Mod. Phys. A **28**, 1340011 (2013), arXiv:1301.5893 [nucl-th].
 - [12] Z.-W. Lin, C. M. Ko, B.-A. Li, B. Zhang, and S. Pal, Phys. Rev. C **72**, 064901 (2005), arXiv:nucl-th/0411110.
 - [13] K. Werner, B. Guiot, I. Karpenko, and T. Pierog, Phys. Rev. C **89**, 064903 (2014), arXiv:1312.1233 [nucl-th].

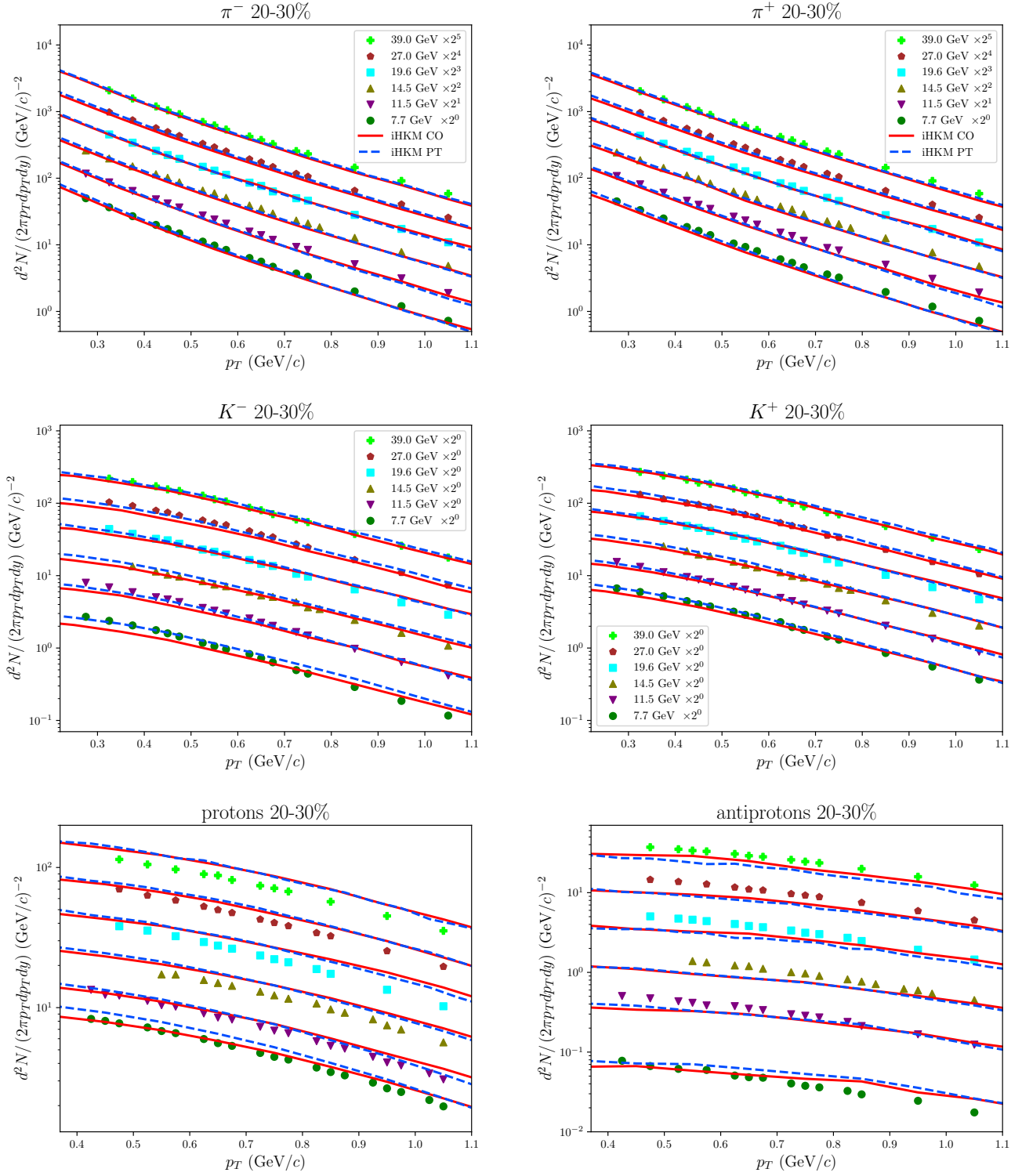


FIG. 4: Comparison of iHKM results with STAR data[45, 46] for π^\pm , K^\pm , p , and \bar{p} in the 20–30% centrality class at midrapidity ($|y| < 0.1$). The pion spectra were used to calibrate the τ_0 and τ_{th} parameters.

[14] C. Shen, Z. Qiu, H. Song, J. Bernhard, S. Bass, and U. Heinz, Comput. Phys. Commun. **199**, 61 (2016), arXiv:1409.8164 [nucl-th].

[15] V. Y. Naboka, I. A. Karpenko, and Y. M. Sinyukov, Phys. Rev. C **93**, 024902 (2016), arXiv:1508.07204 [hep-ph].

[16] M. Adzhymambetov and Y. Sinyukov, Extension of the

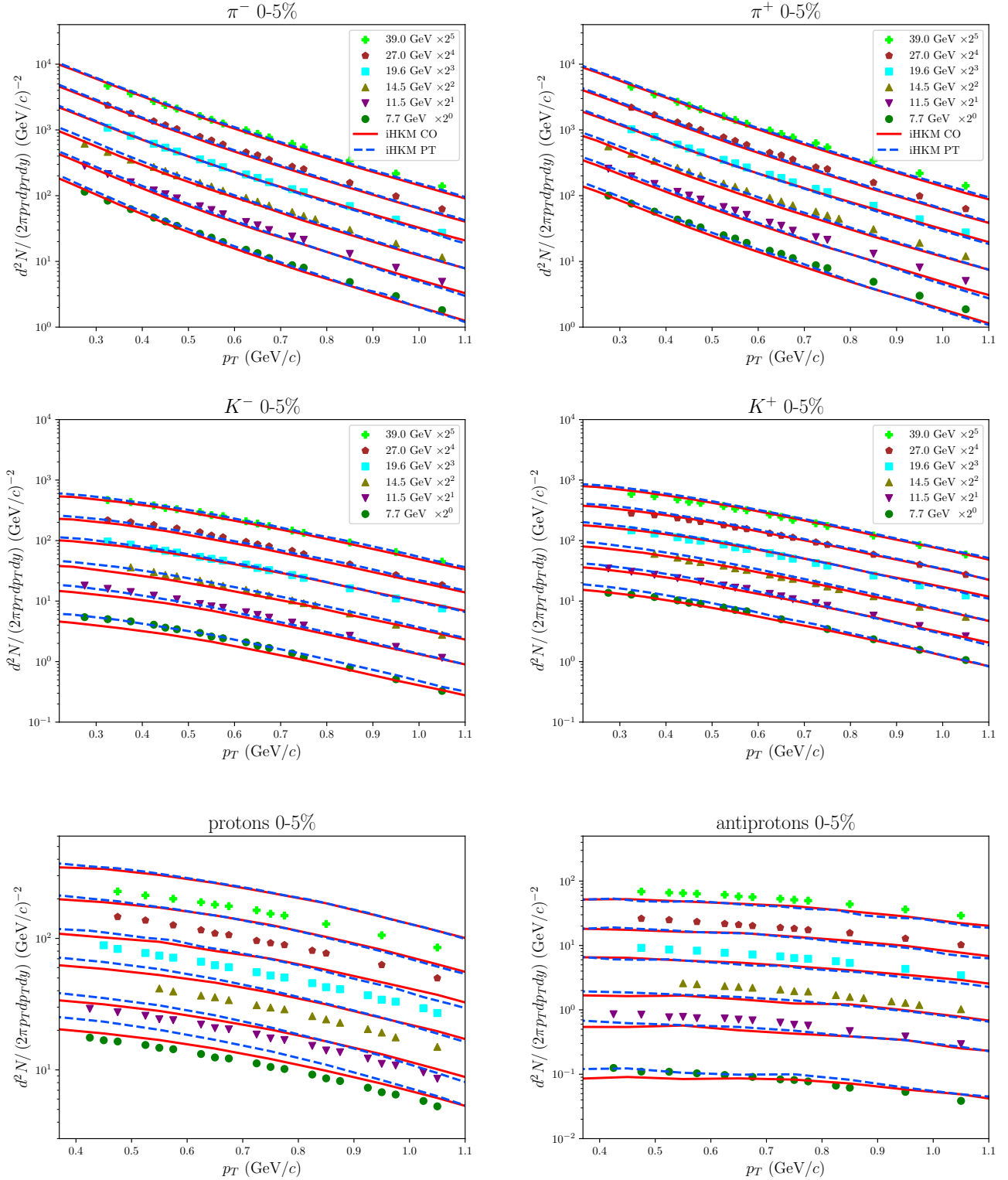


FIG. 5: Comparison of iHKM results with STAR data [45, 46] for π^\pm , K^\pm , p , and \bar{p} in the 0–5% centrality class at midrapidity ($|y| < 0.1$).

integrated HydroKinetic Model to BES RHIC and GSI-FAIR nuclear collision energies (2024), arXiv:2412.00458

[hep-ph].
[17] J. Steinheimer, V. Koch, and M. Bleicher, Phys. Rev. C

- 86**, 044903 (2012), arXiv:1207.2791 [nucl-th].
- [18] C. Shen, G. Denicol, C. Gale, S. Jeon, A. Monnai, and B. Schenke, Nucl. Phys. A **967**, 796 (2017), arXiv:1704.04109 [nucl-th].
- [19] Y. Akamatsu, M. Asakawa, T. Hirano, M. Kitazawa, K. Morita, K. Murase, Y. Nara, C. Nonaka, and A. Ohnishi, Phys. Rev. C **98**, 024909 (2018), arXiv:1805.09024 [nucl-th].
- [20] X.-Y. Wu, G.-Y. Qin, L.-G. Pang, and X.-N. Wang, Phys. Rev. C **105**, 034909 (2022), arXiv:2107.04949 [hep-ph].
- [21] L. Du, U. Heinz, and G. Vujanovic, Nucl. Phys. A **982**, 407 (2019), arXiv:1807.04721 [nucl-th].
- [22] J. Steinheimer, S. Schramm, and H. Stocker, J. Phys. G **38**, 035001 (2011), arXiv:1009.5239 [hep-ph].
- [23] P. F. Kolb and U. W. Heinz, Hydrodynamic description of ultrarelativistic heavy ion collisions, preprint (2003), arXiv:nucl-th/0305084.
- [24] M. Rybczynski, G. Stefanek, W. Broniowski, and P. Bozek, Comput. Phys. Commun. **185**, 1759 (2014), arXiv:1310.5475 [nucl-th].
- [25] W. Florkowski and R. Ryblewski, Phys. Rev. C **83**, 034907 (2011), arXiv:1007.0130 [nucl-th].
- [26] S. V. Akkelin and Y. M. Sinyukov, Phys. Rev. C **81**, 064901 (2010), arXiv:0912.4180 [nucl-th].
- [27] V. Y. Naboka, S. V. Akkelin, I. A. Karpenko, and Y. M. Sinyukov, Phys. Rev. C **91**, 014906 (2015), arXiv:1411.4490 [nucl-th].
- [28] I. Karpenko, P. Huovinen, and M. Bleicher, Comput. Phys. Commun. **185**, 3016 (2014), arXiv:1312.4160 [nucl-th].
- [29] P. Huovinen and H. Petersen, Eur. Phys. J. A **48**, 171 (2012), arXiv:1206.3371 [nucl-th].
- [30] D. Molnar and Z. Wolff, Phys. Rev. C **95**, 024903 (2017), arXiv:1404.7850 [nucl-th].
- [31] A. Monnai, B. Schenke, and C. Shen, Phys. Rev. C **100**, 024907 (2019), arXiv:1902.05095 [nucl-th].
- [32] S. A. Bass *et al.*, Prog. Part. Nucl. Phys. **41**, 255 (1998), arXiv:nucl-th/9803035.
- [33] M. Bleicher *et al.*, J. Phys. G **25**, 1859 (1999), arXiv:hep-ph/9909407.
- [34] H. Petersen, D. Oliinychenko, M. Mayer, J. Staudenmaier, and S. Ryu, Nucl. Phys. A **982**, 399 (2019), arXiv:1808.06832 [nucl-th].
- [35] O. Garcia-Montero, J. Staudenmaier, A. Schäfer, J. M. Torres-Rincon, and H. Elfner, Phys. Rev. C **105**, 064906 (2022), arXiv:2107.08812 [hep-ph].
- [36] O. Savchuk, V. Vovchenko, V. Koch, J. Steinheimer, and H. Stoecker, Phys. Lett. B **827**, 136983 (2022), arXiv:2106.08239 [hep-ph].
- [37] F. Becattini, M. Bleicher, T. Kollegger, M. Mitrovski, T. Schuster, and R. Stock, Phys. Rev. C **85**, 044921 (2012), arXiv:1201.6349 [nucl-th].
- [38] G. Inghirami and H. Elfner, Eur. Phys. J. C **82**, 796 (2022), arXiv:2201.05934 [hep-ph].
- [39] A. Schäfer, I. Karpenko, X.-Y. Wu, J. Hammelmann, and H. Elfner (SMASH), Eur. Phys. J. A **58**, 230 (2022), arXiv:2112.08724 [hep-ph].
- [40] K. Gopal, C. Jena, and K. Nayak, Energy dependence of particle production in Au+Au collisions at $\sqrt{s_{NN}} = 7.7$ -200 GeV using a multiphase transport model (2024), arXiv:2406.13520 [nucl-th].
- [41] J. Cimerman, I. Karpenko, B. Tomasik, and P. Huovinen, Phys. Rev. C **107**, 044902 (2023), arXiv:2301.11894 [nucl-th].
- [42] M. Stefaniak, K. Werner, J. Jahan, and H. P. Zbroszczyk, Phys. Rev. C **108**, 014905 (2023), arXiv:2209.12979 [hep-ph].
- [43] J. Weil *et al.* (SMASH), Phys. Rev. C **94**, 054905 (2016), arXiv:1606.06642 [nucl-th].
- [44] S. A. Jahan, H. Roch, and C. Shen, Phys. Rev. C **110**, 054905 (2024), arXiv:2408.00537 [nucl-th].
- [45] L. Adamczyk *et al.* (STAR), Phys. Rev. C **96**, 044904 (2017), arXiv:1701.07065 [nucl-ex].
- [46] J. Adam *et al.* (STAR), Phys. Rev. C **101**, 024905 (2020), arXiv:1908.03585 [nucl-ex].